Journal of Alloys and Compounds 507 (2010) 526–530

Contents lists available at ScienceDirect

Journal of Alloys and Compounds

journal homepage: www.elsevier.com/locate/jallcom

Supercapacitive properties of ultra-fine MnO_2 prepared by a solid-state coordination reaction

Dao-Lai Fang*, Bing-Cai Wu, Ai-Qin Mao, Yong Yan, Cui-Hong Zheng

School of Materials Science and Engineering, and Anhui Key Laboratory of Metal Materials and Processing, Anhui University of Technology, Ma'anshan, Anhui 243002, PR China

ARTICLE INFO

Article history:
Received 23 May 2010
Accepted 4 August 2010
Available online 12 August 2010

Keywords:
Oxides
Chemical synthesis
Electrochemical measurements
Electrochemical properties

ABSTRACT

An ultra-fine MnO_2 powder was synthesized by a novel route of solid-state coordination reaction. The structure and morphology were characterized by X-ray diffraction, scanning electron microscope and infrared spectroscopy. The MnO_2 powder with a primary particle size of ~200 nm was composed of α-MnO_2 and γ-MnO_2. Electrochemical properties of the MnO_2 electrode were examined by cyclic voltammetry, and galvanostatic charge/discharge and electrochemical impedance spectroscopy measurements in 6 mol L^{-1} KOH electrolyte. The MnO_2 electrode exhibited good supercapacitive performance. Specific capacitance values of 337 and 197 F g^{-1} were obtained for the MnO_2 electrode at scan rates of 2 and 50 mV s^{-1}, respectively. The MnO_2 electrode subjected to 500 cycles at a current density of 800 mA g^{-1} delivered a specific capacitance of 228 F g^{-1}, retaining 75% of its initial specific capacitance.

© 2010 Elsevier B.V. All rights reserved.

1. Introduction

Recently, electrochemical supercapacitors have aroused great interest because they can be used as complementary charge storage devices to conventional batteries in various applications requiring peak power pulses, such as hybrid electric vehicles, nano-electronics, burst power generation, and memory back-up devices [1,2]. Generally the supercapacitors can be classified into two categories: electrical-double-layer capacitors (EDLCs), which build up electrical charge at the electrode/electrolyte interface, and pseudocapacitors, which are based on reversible faradic redox reactions at the interfaces at certain potentials.

Due to its favorable pseudocapacitive characteristics, low cost and environmental friendliness, tetravalent manganese oxide (MnO_2) is a most promising candidate for supercapacitor materials [3,4]. Regardless of its theoretical specific capacitance (SC) as high as 1370 F g^{-1} [5], MnO_2 material prepared so far still exhibits a much lower SC. The powder MnO_2 material prepared by the usual methods such as sol–gel, co-precipitation, thermal decomposition and hydrothermal synthesis possesses a lower SC ranging from 100 to 300 F g^{-1} [6–9]. The film MnO_2 material usually delivers a higher SC, e.g. 698 F g^{-1} for the sol–gel derived film (mass loading ~4 μg cm^{-2}) [10], and 460 F g^{-1} for the electrodeposition derived film [11]. Nevertheless the SC of the film MnO_2 decreases rapidly with increasing film thickness due to its low conductivity. Therefore, it is of great significance to develop an effective preparation method for improving the supercapacitive properties, especially the SC, of the MnO_2 material.

Solid-state coordination reaction route, which lies in between the solid-state and the wet-chemical method in a certain sense, is a very facile yet highly effective method for synthesis of ultra-fine or nanosized particles [12–14]. However, few investigations were reported concerning preparation of MnO_2 material for supercapacitors by this route. In this work, the route was attempted to synthesize manganese oxalate precursor, and a calcination temperature as low as 250 °C was applied to decompose the oxalate precursor for obtaining an ultra-fine MnO_2 powder, which exhibited good supercapacitive performance in terms of the SC and cycle stability.

2. Experimental

2.1. Synthesis of the manganese oxalate precursor and the MnO_2 powder

Analytical-grade manganese acetate $Mn(CH_3COO)_2{\cdot}4H_2O$ and oxalic acid $H_2C_2O_4{\cdot}2H_2O$ were used as starting materials. A powder mixture with a molar ratio of Mn^{2+}:oxalic acid of 1:1 was ball milled at room temperature for 5 h in a polyethylene container using zirconia balls as milling medium. The milled mixture was then dried at 70 °C and calcined for 10 h at 250 °C in air.

2.2. Structural characterization

A Philips X'pert Pro X-ray diffractometer with Cu K_α radiation (λ = 1.5406 Å) was used to analyze the phase compositions of the dried milled mixture and the calcined manganese oxide powder. Diffraction data were collected in the 2θ range from 15° to 70°, using the step-scan mode with a scanning speed of 0.02° step-size and 1 s per step. Fourier transform infrared (FT-IR) spectroscopy of the calcined manganese oxide powder was recorded on a Perkin-Elmer 577 spectrometer with a resolution of ±4 cm^{-1}, using KBr as dispersing medium. The morphology of the

* Corresponding author. Tel.: +86 555 2315318; fax: +86 555 2311570.
E-mail address: fangdl@ustc.edu (D.-L. Fang).

0925-8388/$ – see front matter © 2010 Elsevier B.V. All rights reserved.
doi:10.1016/j.jallcom.2010.08.010

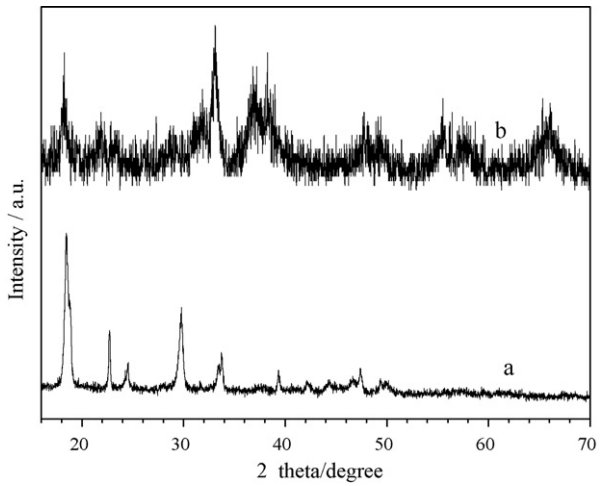

Fig. 1. XRD patterns of the synthesized manganese oxalate (a) and the obtained MnO_2 (b).

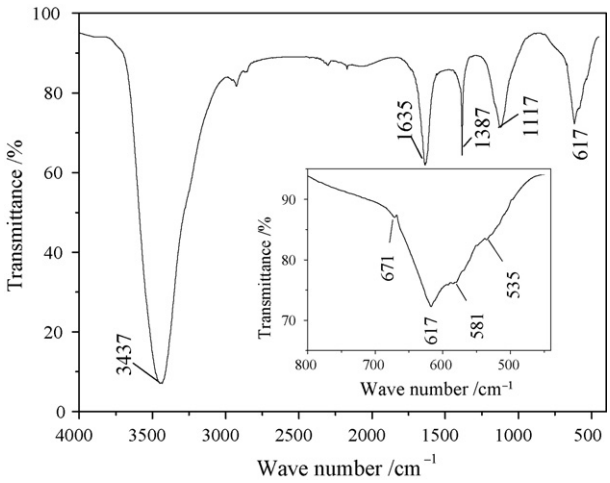

Fig. 2. FT-IR spectra of the obtained MnO_2 powder.

obtained manganese oxide powder was analyzed by using a JSM 6490 scanning electron microscope (SEM).

2.3. Electrode fabrication and electrochemical characterization

The electrodes for electrochemical measurements were composed of the obtained MnO_2, acetylene black (AB) and polytetrafluoroethylene (PTFE), whose weight ratio was 70:25:5. First, the MnO_2 active material and the acetylene black were fully mixed and grinded, then a proper amount of PTFE binder was added into the powder mixture to achieve a homogenous slurry. The prepared slurry was painted onto a nickel foam current collector with an area of 1 cm × 1 cm. Finally, the painted current collector was dried for 10 h at 80 °C, and pressed at a pressure of 10 MPa to form a reliable electrode. Each of the fabricated electrodes contained ~4 mg of the MnO_2 active material.

All the electrochemical measurements concerned were carried out in 6 mol L^{-1} KOH aqueous electrolyte. Cyclic voltammetry measurements were performed on a CHI604C electrochemical workstation in a three-electrode cell set-up, using a MnO_2 electrode fabricated above as the working electrode, a platinum foil as the counter electrode, a saturated calomel electrode (SCE) as the reference electrode. Cyclic voltammograms at different scan rates were recorded between −0.4 and 0.4 V vs. SCE. For evaluation of galvanostatic charge/discharge performance of the MnO_2 electrode, a symmetrical capacitor was assembled by clamping a couple of the identical electrodes separated by a porous polypropylene separator. The galvanostatic charge/discharge performance at different current densities was determined by a battery test system of Neware BTS-3008W in a potential range from 0 to 0.8 V. Electrochemical impedance spectroscopy (EIS) of the MnO_2 electrode was determined with the CHI604C electrochemical workstation, applying an a.c. amplitude of 5 mV in a frequency range of 0.01–10^5 Hz.

3. Results and discussion

3.1. X-ray diffraction patterns and FT-IR spectra of the obtained MnO_2

After the starting materials of manganese acetate and oxalic acid had been ball milled for 5 h, a cream-like, viscous substance was formed, which was then dried at 70 °C, yielding a fine powder of light pink colour. Fig. 1(a) gives XRD pattern of the synthesized manganese oxalate. All the diffraction peaks in Fig. 1(a) are in accordance with those of α-form manganese oxalate (JCPDS: 25-0544), without the characteristic diffraction peaks of the starting materials observed. This suggests that the solid-state coordination reaction between manganese acetate and oxalic acid is completed after ball milling for 5 h, forming a coordination compound of α-form manganese oxalate. For avoiding formation of Mn_2O_3, the synthesized manganese oxalate was calcined in air for 10 h at 250 °C, much lower than its usual nonisothermal decomposition temperature (~300 °C) [15], resulting in a manganese oxide powder of brownish-black colour. Fig. 1(b) represents XRD pattern of the obtained manganese oxide. As shown in Fig. 1(b), the diffraction peaks at $2\theta = 18.2°$, 28.7°, 37.2° and 49.1° well match those of α-MnO_2 (JCPDS: 44-0141), while the peaks at $2\theta = 21.9°$, 33.1°, 38.6°, 57.5°, and 66.0° are in good agreement with those of γ-MnO_2 (JCPDS: 14-0644). This confirms that the obtained manganese oxide is mainly composed of a mixture of α- and γ-MnO_2. Low intensity and broadening of the peaks in Fig. 1(b) indicate that the obtained manganese oxide powder is not well crystallized, and/or that the crystallites in the powder are very fine. The characteristic diffraction peaks of α-form manganese oxalate in Fig. 1(a) are not observed in the XRD patttern in Fig. 1(b), which implies that the isothermal decomposition of the manganese oxalate was completed at a calcination temperature of 250 °C in a duration of 10 h. This conforms to the results given by Mohamed et al. [16], who reported that at heating rate of 5 °C min^{-1} in air, decomposition of anhydrated manganese oxalate was initiated at a temperature as low as 275 °C, and attributed the significant diminishing of the initial decomposition temperature to the role of oxygen in promoting decompositions of transition metal oxalates containing oxidizable cations.

Fig. 2 shows the FT-IR spectra of the obtained MnO_2. The broad absorption band at 3437 cm^{-1} is attributed to the O–H stretching vibration, and the absorption bands observed at 1635, 1387 and 1117 cm^{-1} are usually ascribed to the O–H bending vibrations combined with Mn ions [17]. This suggests that a certain amount of bound water exists in the obtained MnO_2, which is generally believed to be beneficial to the electrochemical activity of MnO_2 materials. The broad absorption bands at 671, 617, 581 and 535 cm^{-1}, as indicated by the inset in Fig. 2, are attributed to the Mn–O vibrations in MnO_6 octahedra of α- and γ-MnO_2 [17–19]. The FT-IR result reveals that the obtained MnO_2 is a mixture of α- and γ-MnO_2 containing a small amount of bound water, which is in line with the XRD result in Fig. 1.

3.2. Morphology of the obtained MnO_2 powder

The morphology of the prepared MnO_2 powder was investigated by scanning electron microscopy (SEM). The lower-magnification SEM image in Fig. 3(a) shows that the prepared MnO_2 powder consists of uniform and spherical particles with a particle size of ~1 μm. The higher-magnification SEM image in Fig. 3(b) discloses that each of the spherical particles observed under lower magnification is actually an agglomerate, which is composed of a number of smaller particles with a particle size of ~200 nm. The solid-state coordination route allows the prepared MnO_2 powder with an ultra-fine particle size, which is mainly related to the unique

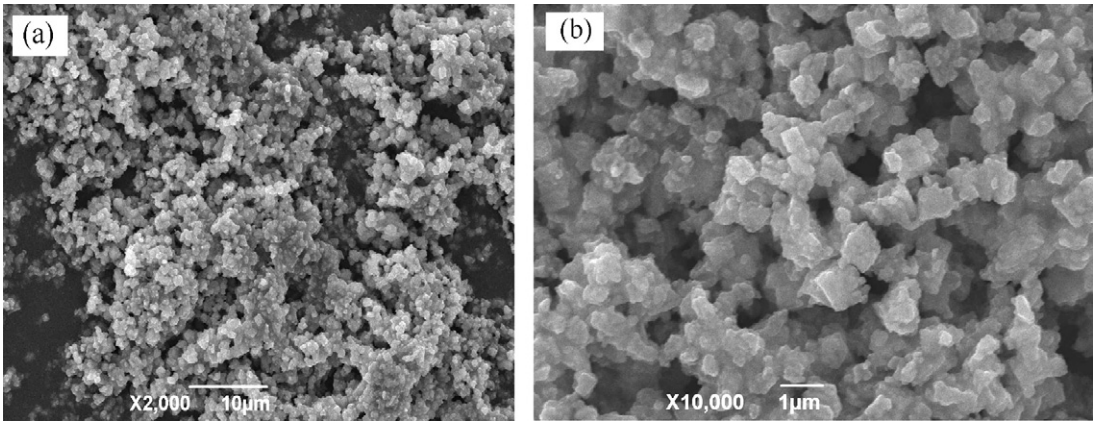

Fig. 3. SEM images of the obtained MnO_2 powder under lower (a) and higher (b) magnification.

conditions of the solid-state coordination reaction, under which the nucleation process is usually much more favorable than the growth process [12,20]. The prepared MnO_2 powder with ultra-fine particles undoubtedly provides a larger effective surface area for redox reactions and cation adsorption/desorption, which is beneficial to promoting its supercapacitive performance.

3.3. Electrochemical properties of the MnO_2 electrode

Cyclic voltammetry (CV) is considered to be an ideal tool to indicate the capacitive behavior of any electrode material. Fig. 4(a) shows the cyclic voltammograms of the MnO_2 electrode measured in a scan rate range from 2 to 50 mV s^{-1} between −0.4 and 0.4 V vs. SCE in 6 mol L^{-1} KOH aqueous electrolyte. Though slightly distorted at higher scan rates, all the cyclic voltammograms obtained are roughly rectangular in shape, suggesting good capacitive behavior of the MnO_2 electrode. Furthermore, all the cyclic voltammograms present a couple of approximately symmetrical current peaks, i.e. an oxidation one around 0.16 V and a reduction one around 0.08 V, which are due to intercalation/detercalation of protons or alkaline metal cations in the MnO_2 electrode in KOH aqueous electrolyte, indicating a considerable faradic pseudocapacitance contribution [21]. The small potential difference between the anodic peak and the cathodic peak, increasing from 0.07 to 0.18 V with increasing scan rates from 2 to 50 mV s^{-1}, reveals the high reversibility of the MnO_2 electrode. The SC of the MnO_2 electrode can be cal-

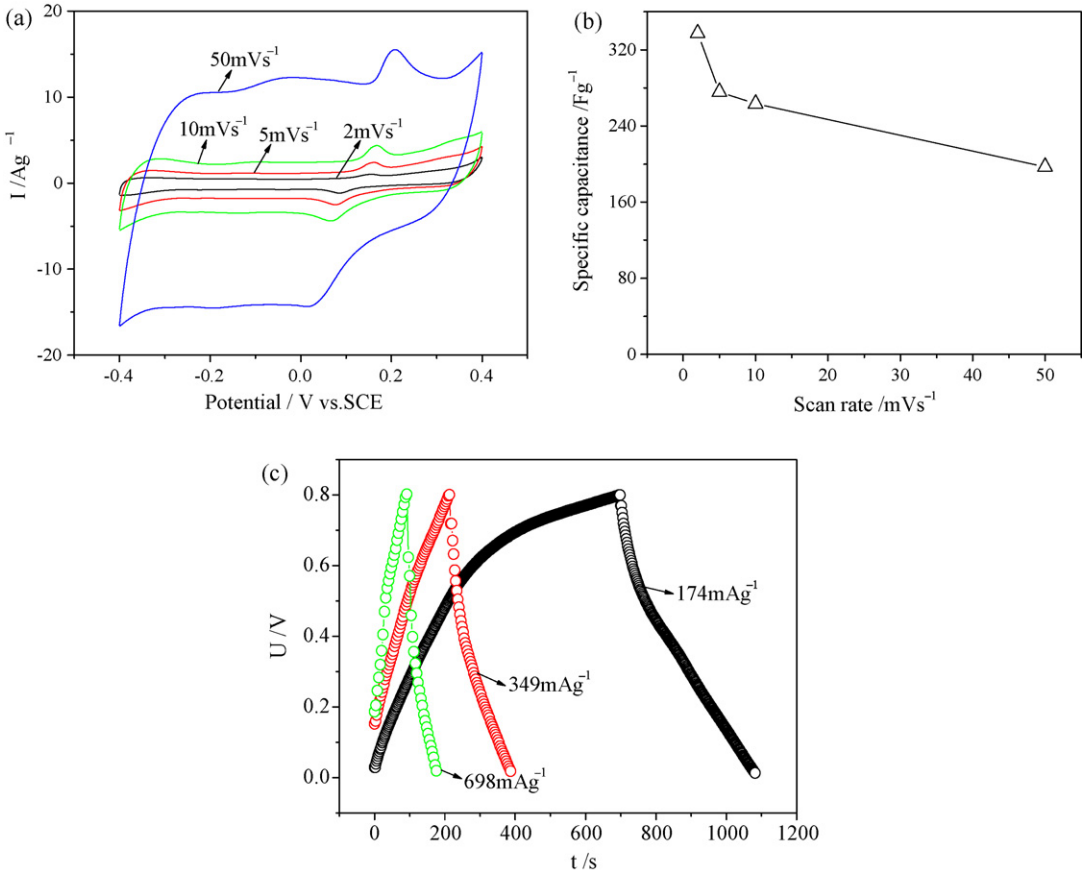

Fig. 4. Cyclic voltammograms with different scan rates (a), scan rate dependence of the SC (b) and galvanostatic charge/discharge profiles at various current densities (c) of the MnO_2 electrode.

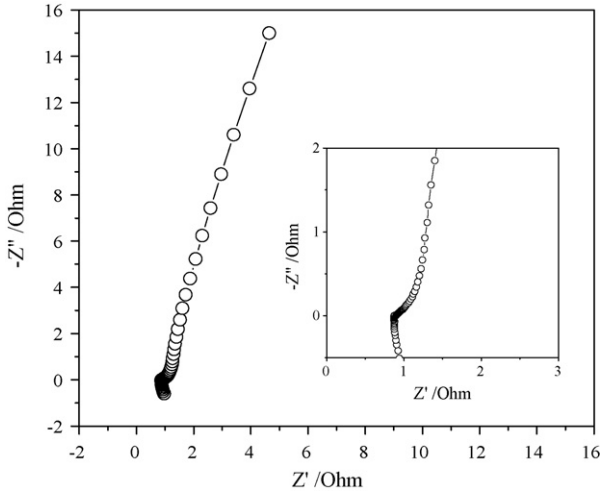

Fig. 5. Electrochemical impedance spectra (EIS) of the MnO_2 electrode in the frequency range of 0.01–10^5 Hz.

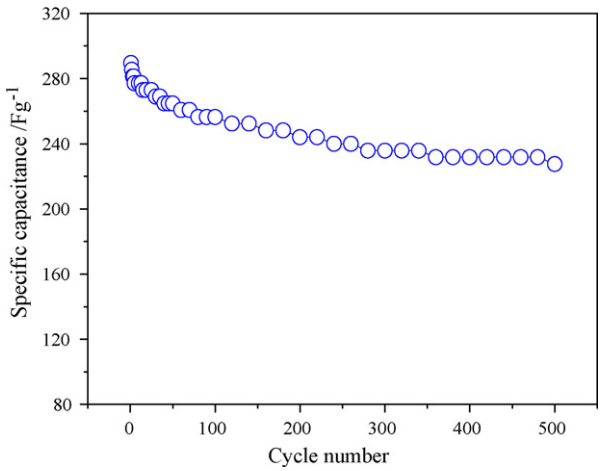

Fig. 6. Cycling life of the MnO_2 electrode at a current density of 800 mA g^{-1} between 0 and 0.8 V.

culated from the cyclic voltammograms according to the formula $C_s = I/m\upsilon$, where C_s is the SC (F g^{-1}), m the mass (g) of the electroactive material, υ the potential scan rate (V s^{-1}), and I the even current response (A) defined by $I = 1/(2(V_c - V_a)) \oint idV$ (V_a and V_c represent the lowest and highest potentials (V), respectively). As shown in Fig. 4(b), the SC of the MnO_2 electrode decreases from 337 to 197 F g^{-1} with increasing scan rates from 2 to 50 mV s^{-1}, which is mainly due to that the redox reactions are based on the intercalation/deintercalation of protons or alkaline metal cations from the electrolyte [9,22]. At lower scan rates, more ions from the electrolyte have a chance to gain access to the electroactive MnO_2 material, and participate in redox reactions, resulting in a higher SC. However, at higher scan rates, the effective interaction between the ions and the electroactive MnO_2 material is decreased accordingly, leading to a lower SC. More importantly, a considerable SC of 197 F g^{-1} was retained even at a higher scan rate of 50 mV s^{-1}, indicating higher power characteristics of the MnO_2 material.

For further investigation of the power properties of the MnO_2 electrode, the galvanostatic charge/discharge profiles at different current densities were determined in an electrochemical window of 0.8 V, as shown in Fig. 4(c). The galvanostatic charge/discharge profiles, especially the ones at lower current densities, are somewhat curved, implying the predominance of the faradic pseudocapacitive nature over the electrical-double-layer capacitive one of the MnO_2 electrode. This result is coincident with the CV result in Fig. 4(a), where a Faradic reaction characteristic, i.e. a couple of redox peaks, could be observed obviously for the MnO_2 electrode. The SC of a symmetrical capacitor, converted to the SC of a single electrode, can be obtained by the formula $C_s = 4I\Delta t/m\Delta V$, where C_s is the discharge SC (F g^{-1}), I the discharge current (A), Δt the discharge time (s), m the total mass (g) of the electroactive material contained in a symmetrical capacitor, ΔV the discharge potential range (V) [23]. The SC of the symmetrical capacitor at current densities of 174, 349 and 698 mA g^{-1} is calculated to be 348, 303 and 293 F g^{-1}, respectively. Significantly, the capacitance degradation is ~16% with increasing current densities from 174 to 698 mA g^{-1}, indicating good rate capability of the MnO_2 electrode.

For further investigation of the actual electrochemical diffusion process, electrochemical impedance spectroscopy (EIS) was performed in the frequency range from 0.01 to 10^5 Hz with an excitation signal of 5 mV, as shown in Fig. 5. The internal resistance R_i of the MnO_2 electrode, consisting of the ionic resistance of electrolyte, the intrinsic resistance of the electroactive material, and the contact resistance at the electroactive material/current collector interface [24], is estimated to be about 0.9 Ω from the point intercepting the real axis in the high frequency range. In the high-medium frequency region, a minor semicircle observed confirms the slight faradic charge-transfer resistance at electrode/electrolyte interface [24,25]. A straight line, nearly vertical to the real axis, appears in the low frequency region, suggesting good capacitive behavior of the prepared MnO_2 electrode. The EIS results are in good agreement with the CV results.

The long-term cycling stability of the MnO_2 electrode was investigated in 6 mol L^{-1} KOH electrolyte by galvanostatic charge/discharge cycling at a current density of 800 mA g^{-1} for consecutive 500 cycles, as shown in Fig. 6. The SC of the prepared MnO_2 electrode fades remarkably during the first 280 cycles, decreasing by ~19% of its initial SC. During the next 220 cycles, the SC of the prepared MnO_2 electrode becomes stable, decreasing by ~6% of its initial SC. A considerable SC of 228 F g^{-1}, about 75% of its initial SC, is still retained for the prepared MnO_2 electrode after 500 cycles, suggestive of good electrochemical stability, which is of practical importance.

4. Conclusion

An ultra-fine MnO_2 powder with a particle size of ~200 nm was prepared by a facile and low-cost method, i.e. calcining the solid-state coordination derived manganese oxalate for 10 h at 250 °C in air. The XRD results showed that the prepared MnO_2 powder was a mixture of poorly crystallized α- and γ-MnO_2. Its electrochemical properties were characterized by CV, galvanostatic charge/discharge cycling, and EIS measurements in 6 mol L^{-1} KOH aqueous electrolyte. The MnO_2 electrode exhibited good supercapacitive performance, delivering a maximum SC of 337 F g^{-1} at a scan rate of 2 mV s^{-1}, and retaining a considerable SC of 197 F g^{-1} even at a scan rate of 50 mV s^{-1}. Furthermore, a SC of 228 F g^{-1}, i.e. 75% of the initial SC, was remained after 500 cycles at a current density of 800 mA g^{-1}, suggesting good electrochemical stability of the prepared MnO_2 electrode. Thus the ultra-fine MnO_2 powder obtained from the solid-state coordination reaction route is a promising material for supercapacitors.

Acknowledgements

This work is financially supported by the Natural Science Foundation of Education Commission of Anhui Province under Grant No. KJ2008A003 and Grant No. KJ2009B050. The financial support provided by the Innovation Project of Anhui University of Technology is gratefully acknowledged.

References

[1] B.E. Conway, Electrochemical Supercapacitors, Kluwer Academic Publishers, New York, 1999, pp. 1–625.
[2] A. Burke, J. Power Sources 91 (2000) 37–50.
[3] T. Brousse, D. Bélanger, Electrochem. Solid-State Lett. 6 (2003) A244–A248.
[4] J.K.W. Chang, T. Tsai, J. Electrochem. Soc. 150 (2003) A1333–A1338.
[5] S. Devaraj, N. Munichandraiah, Electrochem. Solid-State Lett. 8 (2005) A373–A377.
[6] N. Tang, X.-K. Tian, C. Yang, Z.-B. Pi, Mater. Res. Bull. 44 (2009) 2062–2067.
[7] M. Toupin, T. Brousse, D. Belanger, Chem. Mater. 14 (2002) 3946–3952.
[8] V. Subramanian, H.-W. Zhu, R. Vajtai, P.M. Ajayan, B.-Q. Wei, J. Phys. Chem. B. 109 (2005) 20207–20214.
[9] R.N. Reddy, R.G. Reddy, J. Power Sources 124 (2003) 330–337.
[10] S.C. Pang, M.A. Anderson, T.W. Chapman, J. Electrochem. Soc. 147 (2000) 444–450.
[11] B. Dong, T. Xue, C.L. Xu, H.L. Li, Micropor. Mesopor. Mat. 112 (2008) 627–631.
[12] F. Li, J.Q. Xu, X.H. Yu, L.Y. Chen, X.Q. Xin, Sensors Actuat. B 81 (2002) 165–169.
[13] D.L. Fang, Z.B. Wang, P.H. Yang, W. Liu, C.S. Chen, J. Am. Ceram. Soc. 89 (2006) 230–235.
[14] A.B. Yuan, X.L. Wang, Y.Q. Wang, J. Hu, Electrochim. Acta 54 (2009) 1021–1026.
[15] B. Donkova, D. Mehandjiev, Thermochim. Acta 421 (2004) 141–149.
[16] A.M. Mohamed, K.G. Andrew, A.H. Samih, Thermochim. Acta 429 (2005) 57–72.
[17] Z.H. Ai, L.Z. Zhang, F.H. Kong, H. Liu, W.T.J. Xing, R. Qiua, Mater. Chem. Phys. 111 (2008) 162–167.
[18] C.M. Julien, M. Massot, C. Poinsignon, Spectrochim. Acta Part A 60 (2004) 689–700.
[19] M.V. Ananth, S. Pethkar, K. Dakshinamurthi, J. Power Sources 75 (1998) 278–282.
[20] X.R. Ye, D.J. Jia, J.Q. Yu, X.Q. Xin, Z. Xue, Adv. Mater. 11 (1999) 941–942.
[21] E. Raymundo-Pinero, V. Khomenko, E. Frackowiak, J. Electrochem. Soc. 152 (2005) 229–235.
[22] M. Toupin, T. Brousse, D. Bélanger, Chem. Mater. 16 (2004) 3184–3190.
[23] J. Li, X.Y. Wang, Q.H. Huang, S. Gamboa, P.J. Sebastian, J. Power Sources 160 (2006) 1501–1505.
[24] M.W. Xu, D.D. Zhao, S.J. Bao, H.-L.J. Li, Solid State Electrochem. 11 (2007) 1101–1107.
[25] S.S. Zhang, K. Xu, T.R. Jow, Electrochim. Acta 49 (2004) 1057–1061.